Silafluorene as a promising core for cell-permeant, highly bright and two-photon excitable fluorescent probes for live-cell imaging

Marie Auvray, Frédéric Bolze, Gilles Clavier, Florence Mahuteau-Betzer

▶ **To cite this version:**

Marie Auvray, Frédéric Bolze, Gilles Clavier, Florence Mahuteau-Betzer. Silafluorene as a promising core for cell-permeant, highly bright and two-photon excitable fluorescent probes for live-cell imaging. Dyes and Pigments, 2021, 187, pp.109083. 10.1016/j.dyepig.2020.109083 . hal-03330417

HAL Id: hal-03330417
https://hal.science/hal-03330417

Submitted on 31 Aug 2021

HAL is a multi-disciplinary open access archive for the deposit and dissemination of scientific research documents, whether they are published or not. The documents may come from teaching and research institutions in France or abroad, or from public or private research centers.

L'archive ouverte pluridisciplinaire **HAL**, est destinée au dépôt et à la diffusion de documents scientifiques de niveau recherche, publiés ou non, émanant des établissements d'enseignement et de recherche français ou étrangers, des laboratoires publics ou privés.

Silafluorene as a promising core for cell-permeant, highly bright and two-photon excitable fluorescent probes for live-cell imaging

Marie Auvray[a,b], Frédéric Bolze[c], Gilles Clavier[d], Florence-Mahuteau-Betzer[a,b,*]

a Institut Curie, PSL University, CNRS, Inserm, UMR9187-U1196, 91405 Orsay, France
b Université Paris-Saclay, CNRS, Inserm, UMR9187-U1196, 91405, Orsay, France
c Faculté de pharmacie, UMR7199, 67401 Illkirch-Graffenstaden Cedex, France
d PPSM, CNRS, ENS Paris-Saclay, 91190 Gif-sur-Yvette

* Corresponding author F. Mahuteau-Betzer *E-mail address:* florence.mahuteau@curie.fr

Keywords: Fluorescent probes; Silafluorene; Two-photon absorption; Live-cell imaging

Abstract

In this study, we report the synthesis, linear and non-linear photophysical studies and live cell imaging of two two-photon activatable probes based on a silafluorene core: **SiFluo-V** and **SiFluo-L**. Thanks to their quadrupolar (A-*π*-D-*π*-A) design, these probes exhibit respectively good to impressive two-photon cross sections (from 210 GM to 2150 GM). TD-DFT calculations support the experimental evidence that **SiFluo-L** displays far better two-photon absorption properties than **SiFluo-V**. Moreover, **SiFluo-L** possesses all requirements for bioimaging as it is water soluble, cell-permeant and and presents a low cytotoxicity (IC_{80}≥10 µM). It labels mitochondria in live-cell imaging at low laser power with high brightness, contrast and photostability. This study demonstrates that silafluorene is a promising core to develop new two-photon fluorophores for live cell imaging.

1. Introduction

Despite the growing interest on the development of fluorophores for live cell imaging, challenges to be tackled still remain. [1-4] An ideal fluorescent probe for bioimaging should be water-soluble, cell permeant, photostable and should absorb and emit at wavelengths compatible with live cell imaging, with a high fluorescence quantum yield. Two-photon excitation (2PE) offers a great opportunity as it allows excitation wavelengths in the NIR window where the absorption and diffusion of light by biological samples are minimized. This primordial advantage provides the capability to image deep inside a tissue and avoids autofluorescence as endogeneous fluorophores are not excited by two-photon excitation or only following very specific protocols. [5] Moreover, 2PE is confined to a small volume at the focal point of the optical system using a fs pulsed laser. Thus, it provides high spatial resolution and limits excitation of the sample reducing photodamages and photobleaching. Furthermore, 2PE requires a lower photon energy compared to one photon excitation and should therefore be less damaging to cells. Unfortunately, most of the available dyes used for two-photon imaging are not designed and optimized for 2PE microscopy. As these dyes do not possess high absorption cross-sections, their imaging by two-photon microscopy requires a high laser power and therefore induces photodamages anyway. Considerable efforts have been carried out to design new fluorophores with high two-photon absorption abilities but the challenge is to strike the right balance between good photophysical properties and the ability to enter the cells. [6] Molecular engineering of two-photon chromophores led to the identification of π-conjugated quadrupolar systems (D-π-A-π-D or A-π-D-π-A) or octupolar systems as excellent two-photon absorbers. [7] Indeed, the increase of symmetrical internal charge transfer and the dimensionality of the molecule improves the two-photon absorption abilities. [8-9] However, strong 2P absorbers are usually extended aromatic structures with high molecular weight and most of them are not biocompatible as they are not water-soluble. Therefore, there is still a strong interest in the development of new scaffolds for 2PE live cell imaging. Another important criterion for an ideal fluorophore

for live cell imaging is the high signal-to-noise ratio. Fluorescent turn-on probes fulfill this criterion as they restore their fluorescence through a fluorogenic reaction with cellular analytes (metals, thiols, ROS) [10-11] or through immobilization/binding to their biological targets. [1, 12] The unbound or unreacted probe is not fluorescent and this improves the sensitivity of the probe by reducing the background signal. Styryl dyes are known to be fluorescent OFF-ON probes for cellular organelles or biomolecules. [13-15] In previous papers, our laboratory described the synthesis and optical properties of divinylpyridinium carbazoles [16] or triphenylamines [17] as 2PE fluorescent DNA probes suitable for fixed cell imaging. These quadrupolar structures were efficient two-photon absorbers and were water-soluble and cell permeant thanks to their pyridinium moieties. Recently, silicon containing organic molecules were of growing emphasis for the design of fluorescent dyes for bioimaging. For example, silicon containing xanthene dyes were successfully developed for in vivo tumor imaging, triple-color imaging of neuronal activity in mouse brain slices, live cell protein labeling for super-resolution microscopy, calcium imaging and so on. [18-20] Surprisingly, very few work was done on the non-linear properties of such molecules, such as their two-photon absorption capabilities. Thus, a silicon-rhodamine based two-photon fluorescent probe for nitric oxide was recently described with two-photon brightness of 75 GM at 820 nm. [21]

Taking into account the above criteria, we report herein a new class of divinylpyridinium based on a 9-silafluorene core. This silicon-bridge analog of fluorene has been mainly used for the development of organic light-emitting diodes. [22-24] Indeed, silafluorene are much more thermostable than fluorene. Moreover, due to a σ*(Si-C)-π * hyperconjugation effect, the incorporation of silicon atoms into π-conjugated systems is expected to decrease the LUMO energy levels. Thus, a red-shift in absorption can be observed by replacing carbon atom with silicon atom in fluorene. [25] Synthesis of V-shaped SiFluo-V and linear SiFluo-L substituted silafluorenes was successfully carried out. Both one photon and two-photon photophysical properties were evaluated. These dyes were emissive (from 450-650 nm) in water with good fluorescence quantum yields. Their fluorescence was enhanced when they were immobilized in a viscous solvent suggesting a turn-on probe behavior in cells. Moreover, SiFluo-L displayed high two-photon absorption abilities in the 750-800 nm range leading to an efficient emitting probe for 2PE cell imaging.

2. Experimental section

2.1 General procedures

Reagents were purchased as reagent-grade and used without further purification unless otherwise stated. THF and DCM were freshly distilled before use. Analytical thin-layer chromatographies (TLC) were carried out on Macherey Nagel Alugram Xtra SIL G/UV254 plates using UV light (λ = 254 nm) as visualizing agent. Flash chromatographies were carried out with Macherey Nagel silica gel (40-63 µm) or on CombiFlash Companion from Teledyne Isco equipped with packed silica cartridges from Macherey Nagel. Yields refer to chromatographically and spectroscopically pure compounds. NMR spectra were recorded on Bruker AV300 spectrometer at room temperature. Chemical shifts (δ), which are expressed in part per million (ppm), were determined relative to residual non-deuterated solvent as an internal reference respectively $CDCl_3$ and $(CD_3)_2SO$ (^{13}C NMR: δ = 77.23; 39.52 ppm; ^{1}H NMR: δ = 7.26; 2.50 ppm). Coupling constant(s) in hertz (Hz) were measured from one-dimensional spectra and multiplicities were abbreviated as following: s (singlet), d (doublet), t (triplet), q (quadruplet), m (multiplet). MS spectra were recorded on a Waters Micromass ZQ instrument (source voltage 30 kV).

2.2 Synthesis

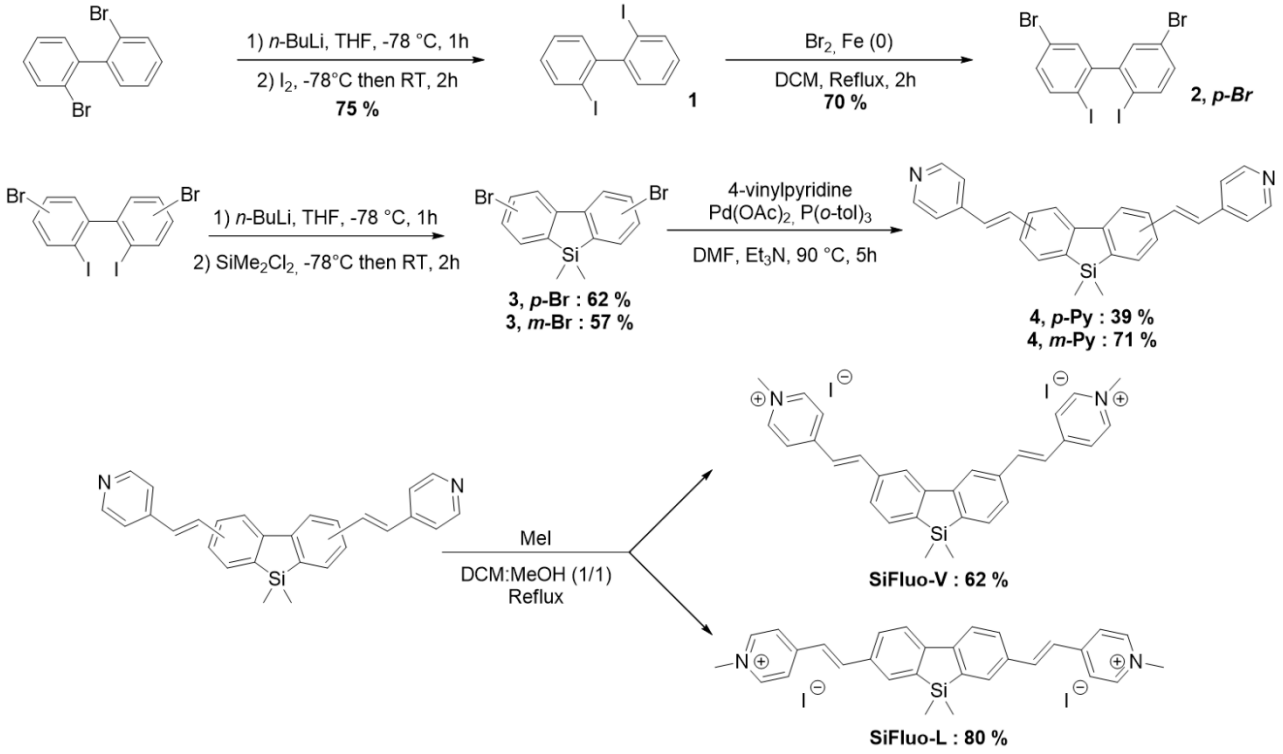

Figure 1. Synthesis of **SiFluo-V** and **SiFluo-L**

*2.2.1 Synthesis of 2,2'-diiodobiphenyl **1:***

At -78 °C and under Ar atmosphere*, n*-BuLi in hexanes (28.0 mL, 1.45 M, 40.5 mmol, 2.3 eq.) was added over 1 hr to a solution of 2,2'-dibromobiphenyl (5.5 g, 17.6 mmol, 1.0 eq.) in dry THF (30 mL). A solution of I_2 (10.3 g, 40.5 mmol, 2.3 eq) in dry THF was then added dropwise. The mixture was allowed to warm to room temperature and stirred for 2 hours. A 2 % sodium thiosulfate aqueous solution (100 mL) was used to quench the reaction. The aqueous layer was extracted three times with DCM. Organic layers were combined, washed with brine and dried over $MgSO_4$. The crude was filtered over a small silica plug (Eluent: Cyclohexane) and after concentration, the filtrate was recrystallized in pure heptane to afford the expected product as white crystals (5.40 g, 13.3 mmol, η **= 75 %**). **CAS number** [2236-52-4] **^{1}H NMR** (300 MHz, $CDCl_3$): δ = 7.95 (dd, J = 7.5 Hz, J = 1.0 Hz, 2H), 7.42 (td, J = 7.5 Hz, J = 1.0 Hz, 2H), 7.20 (dd, J = 7.5 Hz, J = 1.5 Hz, 2H), 7.09 (td, J = 7.5 Hz, J = 1.5 Hz, 2H). Spectroscopic data were in agreement with those reported in the literature. [26]

*2.2.2 Synthesis of 5,5'-dibromo-2,2'-diiodobiphenyl **2, p-Br:***

Under Ar atmosphere, Br_2 (1.43 mL, 27.8 mmol, 2.2 eq.) and iron (106 mg, 1.9 mmol, 0.2 eq.) were added to a solution of 2,2'-diiodobiphenyl **1** (5.15 g, 12.6 mmol, 1.0 eq) in dry DCM (120 mL). The mixture was heated under reflux 2 hours, a 2 % aqueous sodium thiosulfate solution (100 mL) was then used to quench the reaction. The aqueous layer was extracted three times with DCM. Organic layers were combined, washed with brine and dried over $MgSO_4$. The crude was washed with DCM and filtered to afford the expected product as a white powder (5.00 g, 8.87 mmol, η **= 70 %**). **CAS number** [852139-02-7] **^{1}H NMR** (300 MHz, $CDCl_3$): δ = 7.78 (d, J = 8.5 Hz, 2H), 7.32 (d, J = 2.5 Hz, 2H), 7.24 (dd, J = 8.5 Hz, J = 2.5 Hz, 2H). Spectroscopic data were in agreement with those reported in the literature. [26]

*2.2.3 Synthesis of 2,8-dibromo-5,5-dimethyl-5H-dibenzo[b,d]silole **3, p-Br:***

At -78 °C and under Ar atmosphere, *n*-BuLi in hexanes (5.81 mL, 1.45M, 8.42 mmol, 2.0 eq.) was added over 1 hr to a solution of 5,5'-dibromo-2,2'-diiodobiphenyl ***2, p*-Br** (2.38 g, 4.21 mmol, 1.0 eq.) in dry THF (80 mL). After 30 min, dichlorodimethysilane (770 μL, 6.32 mmol, 1.5 eq.) was added dropwise. The mixture was then allowed to warm to room temperature and stirred for 2 hours. Water (100 mL) was introduced to quench

the reaction. The aqueous layer was extracted three times with DCM. Organic layers were combined, washed with brine and dried over $MgSO_4$. The crude was filtered over a small silica plug (Eluent: Cyclohexane) and the filtrate was concentrated under reduce pressure. The resulting residue was washed with pentane and filtered to afford the expected product as white crystals (0.96 g, 2.61 mmol, η **= 62 %**). **CAS number** [1315321-81-3]. **^{1}H NMR** (300 MHz, $CDCl_3$): δ = 7.90 (d, J = 1.5 Hz, 2H), 7.48 (d, J = 7.5 Hz, 2H), 7.43 (dd, J = 1.5 Hz, J = 7.5 Hz, 2H), 0.41 (s, 6H). **^{13}C NMR** (75 MHz, $CDCl_3$): δ = 148.7, 137.9, 134.2, 130.9, 125.5, 124.6, -3.3. **TLC**: Rf (Cyclohexane) = 0.59

2.2.4 Synthesis of 3,7-dibromo-5,5-dimethyl-5H-dibenzo[b,d]silole ***3, m*-Br*:***

According to the same procedure, *n*-BuLi in hexanes (0.49 mL, 1.45 M, 0.71 mmol, 2.0 eq.), 4,4'-dibromo-2,2'-diiodobiphenyl (200 mg, 0.35 mmol, 1.0 eq.) and dichlorodimethysilane (65 μL, 0.53 mmol, 1.5 eq.) in dry THF (6 mL) led to the expected product as white crystals (75 mg, 0.20 mmol, η **= 57 %**). **CAS number** [1228595-79-6]. **^{1}H NMR** (300 MHz, $CDCl_3$): δ = 7.71 (d, *J* = 2.0 Hz, 2H), 7.63 (d, *J* = 8.5 Hz, 2H), 7.54 (dd, *J* = 8.5, 2.0 Hz, 2H), 0.43 (s, 6H). **^{13}C NMR** (75 MHz, $CDCl_3$): δ = 145.6, 141.5, 135.7, 133.4, 122.6, 122.5, -3.4. **TLC**: Rf (Cyclohexane) = 0.68. Spectroscopic data were in agreement with those reported in the literature. [24]

2.2.5 Synthesis of 4,4'-((1E,1'E)-(5,5-dimethyl-5H-dibenzo[b,d]silole-2,8-diyl)bis(ethene-2,1-diyl))dipyridine ***4, p*-Py*:***

Under Ar atmosphere, a solution of $Pd(OAc)_2$ (3 mg, 14 μmol, 0.1 eq.) and P(*o*-tol)$_3$ (6.5 mg, 21 μmol, 0.2 eq.) in a freshly degassed Et_3N/DMF mixture (2:1, 2 mL) was stirred 15 min and degassed once again. Intermediate **3, *p*-Br** (52 mg, 0.14 mmol, 1.0 eq.) and 4-vinylpyridine (0.04 mL, 0.35 mmol, 2.5 eq.) were added. The mixture was then stirred at 90 °C overnight. The crude was diluted in DCM (25 mL). The organic layer was washed with saturated $NaHCO_3$ and dried over $MgSO_4$. The crude was purified by flash chromatography on silica gel (DCM/EtOH 100:0 to 90:10). The resulting solid was dissolved in DCM. Diethyl ether was added until precipitation of a white solid. The precipitate was filtered under vacuum to afford the expected product as a white powder (23 mg, 55 μmol, η **= 39 %**). **^{1}H NMR** (300 MHz, $CDCl_3$): δ = 8.62 (d, J = 6.0 Hz, 4H), 8.05 (s, 2H), 7.68 (d, J = 7.5 Hz, 2H), 7.50 (d, J = 7.5 Hz, 2H), 7.43 (d, J = 6.0 Hz, 4H), 7.42 (d, J = 16.5 Hz, 2H), 7.18 (d, J = 16.5 Hz, 2H), 0.46 (s, 6H). **^{13}C NMR** (75 MHz, $CDCl_3$): δ = 150.4, 148.1, 144.6, 140.4, 138.2, 133.5, 133.4, 126.7, 126.5, 121.0, 119.3, -3.1. **MS** (ES+): m/z = 417.3. **HRMS** (ES+): calculated for $C_{28}H_{25}N_2Si^+$ 417.1787, found 417.1784. **TLC**: Rf (DCM/EtOH, 95:5) = 0.21

2.2.6 Synthesis of 4,4'-((1E,1'E)-(5,5-dimethyl-5H-dibenzo[b,d]silole-3,7-diyl)bis(ethene-2,1-diyl))dipyridine ***4, m*-Py*:***

According to the same procedure, $Pd(OAc)_2$ (4 mg, 18 μmol, 0.1 eq.), P(*o*-tol)$_3$ (8 mg, 26 μmol, 0.15 eq.) , intermediate **3, *m*-Br** *(*65 mg, 0.18 mmol, 1.0 eq.) and 4-vinylpyridine (47 μL, 0.44 mmol, 2.5 eq.) in a Et_3N/DMF mixture (2:1, 3 mL) led to the expected product as a yellow solid (52 mg, 0.12 mmol, η **= 71 %**).**^{1}H NMR** (300 MHz, $CDCl_3$): δ = 8.58 (d, *J* = 6.0 Hz, 4H), 7.83 (s, 2H), 7.81 (d, *J* = 8.0 Hz, 2H), 7.60 (dd, *J* = 8.0, 1.5 Hz, 2H), 7.37 (d, *J* = 6.0 Hz, 4H), 7.34 (d, *J* = 16.0 Hz, 2H), 7.07 (d, *J* = 16.0 Hz, 2H), 0.50 (s, 6H). **^{13}C NMR** (75 MHz, $CDCl_3$): δ = 150.4, 148.0, 144.8, 140.1, 135.5, 133.1, 131.5, 129.5, 125.8, 121.6, 120.9, -3.1. **MS** (ES+): m/z = 417.4. **HRMS** (ES+): calculated for $C_{28}H_{25}N_2Si^+$ 417.1787, found 417.1779 **TLC**: Rf (DCM/EtOH, 95:5) = 0.31

2.2.7 Synthesis of ***SiFluo-V****:*

A large excess of iodomethane (0.3 mL, 100 eq.) was added to a solution of compound **4, *p*-Py** (20 mg, 48 μmol, 1.0 eq.) in a MeOH/DCM (1:1) mixture (2 mL). The reaction was stirred at 30 °C overnight. After addition of diethyl ether, the yellow precipitate was filtered under vacuum to afford the expected product as a pale yellow solid (21 mg, 30 μmol, η **= 62 %**).**^{1}H NMR** (300 MHz, DMSO-d_6): δ = 8.92 (d, *J* = 6.0 Hz, 4H), 8.63 (s, 2H), 8.35 (d, *J* = 6.0 Hz, 4H), 8.12 (d, *J* = 16.5 Hz, 2H), 7.98 (d, *J* = 16.5 Hz, 2H), 7.88 (d, *J* = 7.5 Hz, 2H), 7.65 (d, *J* = 7.5 Hz, 2H), 4.29 (s, 6H), 0.46 (s, 6H). **^{13}C NMR** (75 MHz, DMSO-d_6): δ = 152.4, 147.5, 145.2, 141.8, 140.5, 137.4, 133.9, 128.5, 124.0, 123.6, 119.7, 47.0, -3.4. **MS** (ES+): m/z = 445.3. **HRMS** (ES+): calculated for $C_{30}H_{30}N_2ISi^+$ 573.1223, found 573.1250

*2.2.8 Synthesis of **SiFluo-L**:*

According to the same procedure, iodomethane (0.35 mL, 100 eq.) and compound **4, *m*-Py** (20 mg, 48 μmol, 1.0 eq.) in a MeOH/DCM (1:1) mixture (2 mL) led to the expected product as an orange solid (31 mg, 44 μmol, η **= 80 %**).**^{1}H NMR** (300 MHz, DMSO-d_6): δ = 8.86 (d, *J* = 6.5 Hz, 4H), 8.22 (d, *J* = 6.5 Hz, 4H), 8.19 (d, *J* = 1.0 Hz, 2H), 8.13 (d, *J* = 8.0 Hz, 2H), 8.06 (d, *J* = 16.0 Hz, 2H), 7.85 (dd, *J* = 8.0, 1.0 Hz, 2H), 7.60 (d, *J* = 16.0 Hz, 2H), 4.26 (s, 6H), 0.50 (s, 6H). **^{13}C NMR** (75 MHz, DMSO-d_6): δ = 152.4, 148.5, 145.1, 140.4, 140.1, 134.7, 132.6, 131.1, 123.4, 123.1, 122.3, 46.9, -3.4. **MS** (ES+): m/z = 445.1. **HRMS** (ES+): calculated for $C_{30}H_{30}N_2ISi^+$ 573.1223, found 573.1227

2.3 Optical measurements

Measurements were performed in 0.5 or 1 mL Hellma quartz cuvette (material code QS blue, 200−2000 nm). Fluorescence and UV-visible spectra were respectively recorded using Spex FluoroMax-3 Jobin-Yvon Horiba and Hitachi U-2900 apparatus. Measurements were performed at room temperature with solutions of A < 0.1 to avoid re-absorption of the emitted light, and data were corrected with a blank and from the variations of the detector with the emitted wavelength. Fluorescence quantum yield were measured according to the Crosby method using quinine sulfate (λ_{ex} = 366 nm, Φ = 0.546) as reference. [27-28]

2.4 Molecular Modeling

Geometry optimizations of the ground state were carried out at the B3LYP/6-31G(d) level of theory. A frequency calculation was done in all cases to confirm the true minimum nature (no imaginary frequency) of the converged geometry. TD-DFT calculations were done at the M06-2X/6-311+G(d,p) level of theory using IEFPCM model to include solvent (water) effect. All calculations were done with Gaussian 09 software from Gaussian Inc. and orbitals were plotted with Avogadro.

2.5 Two-photon absorption

The two-photon excitation spectra were measured by the fluorescence method by using a Ti:sapphire femtosecond laser Insight DS (680-1300 nm) with pulse width < 120 fs and a repetition rate of 80 MHz (Spectra-Physics) The excitation beam was collimated over the cell length (Helma fluorescence semi-micro 10x4 mm) and the fluorescence, collected at 90° of the excitation beam, was focused into an optical fibre connected to a spectrometer (AvaSpec ULS from Avantes). The incident beam intensity was adjusted to ensure an intensity-squared dependence of the fluorescence over the whole spectral range reported. To avoid reabsorption of emitted light, micro cells are used and the focal point is very close to the edge of the cuvette. This allows elimination of second order filter effects. The concentrations were 5x10^{-5}M for **SiFluo-L** and 10^{-4}M for **SiFluo-V**. Calibration of the spectra was performed by comparison with the published Rhodamine B in MeOH [29-30] in the 750-880 and 930-1000 nm range and Fluorescein in 0.1N NaOH solution in the 880-930 nm range. [30]

2.6 Cell culture and confocal microscopy imaging

A549 lung carcinoma cells were cultured in Dulbecco's modified eagle media (DMEM, GIBCO) supplemented with 10% Fetal Bovine Serum (FBS, GIBCO) and 1% Penicillin/Streptomycin (Life Technologies) at 37 °C under 5% CO_2, 95 % air and 100 % humidity. Cells were seeded on a 8-well μ-slide from Ibidi (20 000 cells/well). After 24h, cells were incubated 2 hours with the desired compound, washed with PBS once, and observed in Opti-MEM (GIBCO) medium.

For MTT Assay, cells were seeded in 24-well plates from TPP (50 000 cells/well). After 24h, cells were incubated with solutions of various concentrations of both probes (for 0.313 to 10 µM) for 24 hours. Afterwards, 50 µL of MTT solution (previously sterilized with a 0.22 µm filter, 5 mg/mL in PBS) were added in each well. After 1h, the medium was removed and 600 µL of DMSO were added to dissolve MTT formazan. Optical densities were then measured at 562 nm with a FLUOStar Omega plate reader from BMG Labtech.

Every experiment was conducted in duplicate and reproduced three times. Results are represented as means ± SD.

The fluorescence imaging (confocal and biphotonic) was performed using a confocal laser scanning microscope DMI 6000 with a SP5-AOBS unit (both Leica) equipped with a 63x (NA = 1.4) objective (oil immersion), an argon gas laser, a 405 nm diode and helium neon gas laser (633 nm) for one-photon excitation and a Chameleon Ti:Saph laser (Coherent) delivering pulses in the 100 to 200 fs range at an 80 MHz repetition rate with a tunability ranging from 705 to 980 nm for two-photon excitation. The excitation laser power was measured after the objective by a thermal head laser power meter (PM100 S302 ThorLabs). The images were visualized and processed using Image J software (Rasband W.S., U.S. National Institutes of Health, Bethesda, Maryland, USA).

3 Results and discussion

3.1 Synthesis

Compounds SiFluo-V and SiFluo-L were synthesized according to the synthetic pathway shown in Figure 1. A two-step synthesis adapted from a method previously described was performed to afford 5,5'-dibromo-2,2'-diiodobiphenyl 2, p-Br. [26] Halogen-metal exchange on 2,2'-dibromobiphenyl with n-BuLi in THF followed by the addition of iodine afforded 2,2'-diiodobiphenyl 1 in 75 % yield. Compound 1 was then brominated in dichloromethane in the presence of bromine and iron to provide 5,5'-dibromo-2,2'-diiodobiphenyl 2,p-Br in 2 hours in 70 % yield. For the synthesis of SiFluo-L, the starting material 2, m-Br was commercially available. The silafluorene cores were obtained according to a strategy described in the literature starting with compounds 2-Br. [22, 24] Chemoselective halogen-metal exchanges on dibromo-2,2'-diiodobiphenyls 2-Br on iodine atoms with n-BuLi in THF were followed by nucleophilic substitutions on commercial dichlorodimethylsilane. This afforded brominated silafluorenes 3, m-Br and 3, p-Br with good yields, 57 % and 62 % respectively. A Heck reaction in the presence of 4-vinylpyridine was then performed to give 4, m-Py and 4, p-Py. The moderate yield obtained for 4, p-Py (39 %) could be explained by difficulties met in purification steps. Pyridine moieties were finally methylated to yield pyridinium iodide salts SiFluo-V and SiFluo-L. To sum up, SiFluo-V and SiFluo-L were respectively obtained in 8 % overall yield by a five-step synthesis and in 32 % overall yield by a three-step synthesis.

3.2 UV/vis and fluorescent properties

The optical properties of **SiFluo-V** and **SiFluo-L** have been investigated in water (μ = 1,002.10^{-3} Pa.s at 20 °C) and glycerol (μ = 1,420 Pa.s at 20 °C) at room temperature. All data are summarized in **Table 1**. These dyes obey Beer Lambert's law up to 180 µM in water (SI, Figure S1) indicating that they do not aggregate in aqueous media and are highly water soluble.

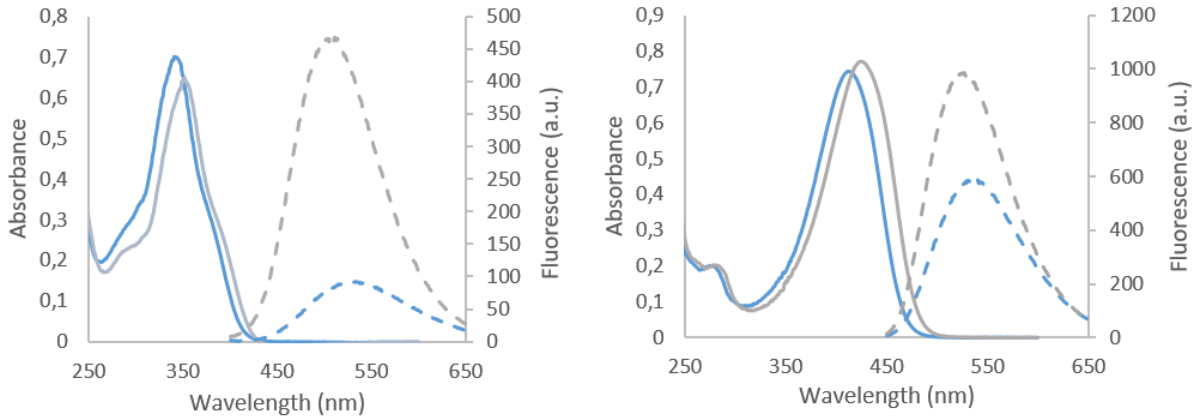

Figure 2. Absorption (12 µM – solid lines) and emission spectra ($\lambda_{ex} = \lambda_{max,}$ 2 µM - dashed lines) of **SiFluo-V** (Left) and **SiFluo-L** (Right) in water (blue lines) and glycerol (grey lines)

SiFluo-V shows an absorbance around 350 nm, whereas SiFluo-L absorbs in the violet region between 416 and 425 m, depending on the solvents (Figure 2 and Table 1). This may reveal a lower degree of conjugation of the V-shaped compound SiFluo-V compared to the linear isomer SiFluo-L originating in its lower rigidity. In addition, SiFluo-V and SiFluo-L exhibit high molar absorption coefficients which are slightly higher for SiFluo-L (up to 64 200 L.mol-1.cm-1 in glycerol). This difference could also be explained by a more rigid structure for SiFluo-L. In spite of the difference of absorption range, both compounds display a green fluorescence in water and in glycerol. Small shifts observed in absorption and emission in the different solvents are consistent with an intramolecular charge transfer (see 3.4). Furthermore, they display large to impressive Stokes shifts, respectively 5000 cm-1 to 10 000 cm-1 for SiFluo-L and SiFluo-V. These Stokes shifts are about 10 times higher than lots of fluorescent probes used for biological purposes like fluorescein, rhodamine, boron-dipyrromethene or cyanines. That represents a real advantage for one photon excitation imaging, avoiding problems like reabsorption and optical setup implementation. Both dyes are emissive in water, SiFluo-L exhibiting a stronger fluorescence in water than SiFluo-V (13 % versus 3 %). This behavior was quite unexpected as we reported previously that N-phenylcarbazole analogue Cbz-2Py was poorly emissive in water (ϕ_F < 0.5%) and restored its fluorescence while binding DNA. [16] In our case, fluorescence could also be enhanced if non-radiative relaxation, such as rotation of the styryl moieties, is inhibited by immobilization inside its cellular target. In order to evaluate the putative increase of fluorescence of SiFluo dyes in a cellular medium, their fluorescent properties were measured in glycerol, a highly viscous solvent (μ = 1.49 Pa.s at 20 °C), that limits the non-radiative relaxation pathways from excited state to ground state through restriction of molecular motions. Both probes exhibit a strong fluorescence in glycerol (ϕ_F = 29 % and 31 %), meaning that these probes are responsive to the constraints of the environment. It may indicate that SiFluo-V and SiFluo-L could exhibit a similar fluorescence in cells, immobilized on their biological target. In addition, both probes show a high and similar brightness in glycerol, which is the figure of merit for imaging. The signal-to-noise ratio could be estimated regarding to the brightness in glycerol compared to the brightness in water. As a consequence, SiFluo-V seems to be a better candidate for bioimaging thanks to its great turn-on properties, but its low absorption wavelength represents a limitation. Overall, these results indicated that SiFluo-V but mostly SiFluo-L thanks to its red-shifted absorption wavelengths, are suitable for cellular imaging.

Compound	Solvent	ε ($L.mol^{-1}.cm^{-1}$)	λ_{max}abs (nm)	λ_{max}em (nm)	Stokes Shift (cm^{-1})	Φ	Brightness εΦ ($L.mol^{-1}.cm^{-1}$)
SiFluo-V	Water	58 600	345	530	10 100	3 %	**1 760**
	Glycerol	54 100	350	510	9 000	31 %	**16 770**
SiFluo-L	Water	62 900	416	535	5 300	13 %	**8 180**
	Glycerol	64 200	425	530	4 700	29 %	**18 610**

Table 1. Photophysical properties of **SiFluo-V** and **SiFluo-L** in water and glycerol

3.3 Two-photon absorption cross-sections

The two-photon absorption properties of **SiFluo-V** and **SiFluo-L** have been investigated in water and glycerol solutions at room temperature. Measures were also performed in DMSO in order to compare them with reported cross-section of analogous fluorenes. [31] All data are summarized in Table 2. **SiFluo-L** exhibits outstanding absorption cross-sections, up to 2150 GM regardless of the solvent used, with a maximum around 750 nm (Figure 3).

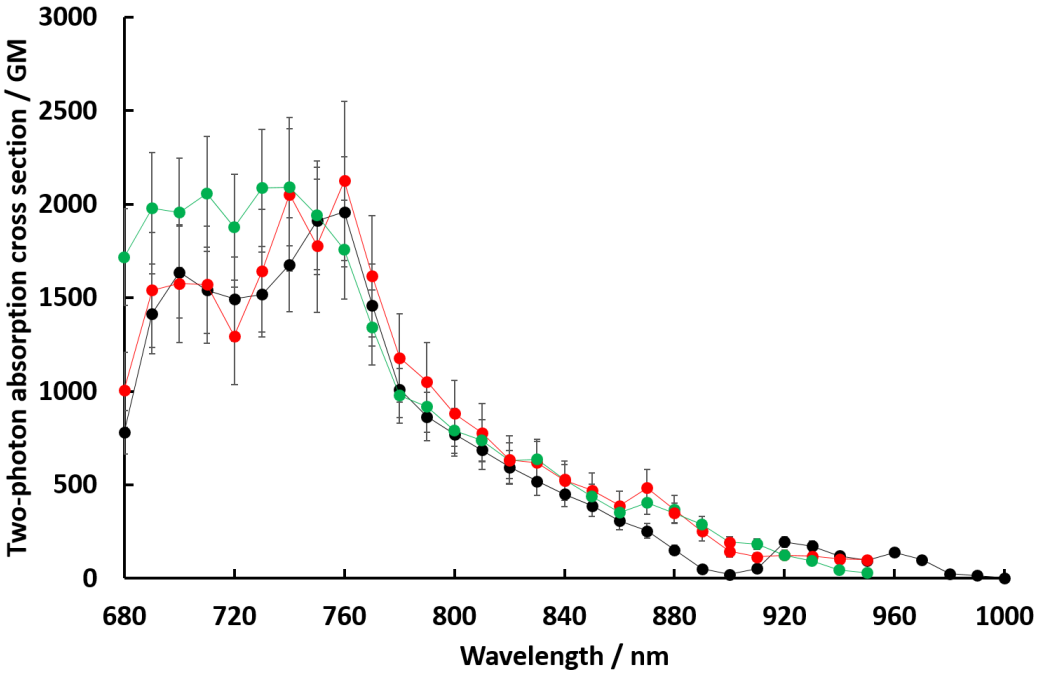

Figure 3. Nonlinear excitation spectra of **SiFluo-L** in water (green), glycerol (red) and DMSO (black)

The two-photon induced fluorescent signal for SiFluo-V was unfortunately too low to be precisely quantified at λ > 680 nm in water and in DMSO. Conversely, cross-section values in glycerol were determined and the maximal cross section was about 210 GM at 700 nm (SI, Figure S2). The TPA cross-section of SiFluo-L is about three times higher than the corresponding fluorene (800 GM at 780 nm, DMSO) [31] but slightly lower than the corresponding carbazole (2 900 GM at 800 nm, water). [32] As for the one photon excitation imaging, the figure of merit for non-linear imaging is the two-photon brightness and not the absorption cross-section. The two-photon brightness of our linear silafluorene in water (270 GM at 740 nm) is higher than the two-photon brightness of the corresponding carbazole (87 GM at 800 nm) and other described silicon containing rhodamine (75 GM at 820 nm). [21, 32] Unfortunately, the brightnesses in glycerol could not be compared as there is no reported data in this solvent for both carbazole and fluorene.

Compound	Solvent	$\lambda_{max,2PA}$ abs (nm)	δ (GM)	Φ	Two-photon brightness δ.Φ (GM)
SiFluo-V	Water	-	nd	3 %	-
	Glycerol	700	210	31 %	**65**
	DMSO	-	nd	1 %	-
SiFluo-L	Water	740	2100	13 %	**270**
	Glycerol	760	2150	29 %	**620**
	DMSO	760	2000	25 %	**500**

Table 2. Two-photon absorption properties of **SiFluo-V** and **SiFluo-L** in water, glycerol and DMSO

3.4 Molecular Modeling

TD-DFT calculations in water (M06-2X/6-311+G(d,p) level of theory) were performed to better understand the photophysical properties of **SiFluo-V** and **SiFluo-L**. For both probes, calculated wavelengths of the maximum absorption are close to experimental values, 424 nm versus 416 nm for **SiFluo-L** and 367 nm versus 345 nm for **SiFluo-V**. The oscillator strengths are similar for **SiFluo-L** (2.62) and **SiFluo-V** (2.79) which is in accordance with their similar extinction coefficients (SI, Table S2). Indeed, for **SiFluo-L**, there is a strong difference in energy between the first calculated transition (424 nm) and the following one (350 nm). At the opposite, in the case of **SiFluo-V**, the transitions are very close to each other (367, 347 and 322 nm) and

therefore they all contribute to the absorption range 280-400 nm of **SiFluo-V**. This agreement between experimental data and calculations allows validating the choice of the computational method.

SiFluo-V possesses a higher LUMO and a lower HOMO than **SiFluo-L**, meaning that the π-conjugation is better for 2,7- than 3,6-substitution. These data are consistent with the redshift observed in the absorption spectrum of **SiFluo-L**. The nature of the transition can be determined looking at shapes of frontiers orbitals (Figure 4). In both cases, the major contribution to the transition from S_0 to S_1 is HOMO → LUMO (SI, Table S1). The electronic density of the HOMO is mostly located on the silafluorene core for the two probes whereas the electronic density of the LUMO is located on the whole structure in both cases. Nevertheless, HOMO-1 and LUMO+1 play also a role in the transition from S_0 to S_1.

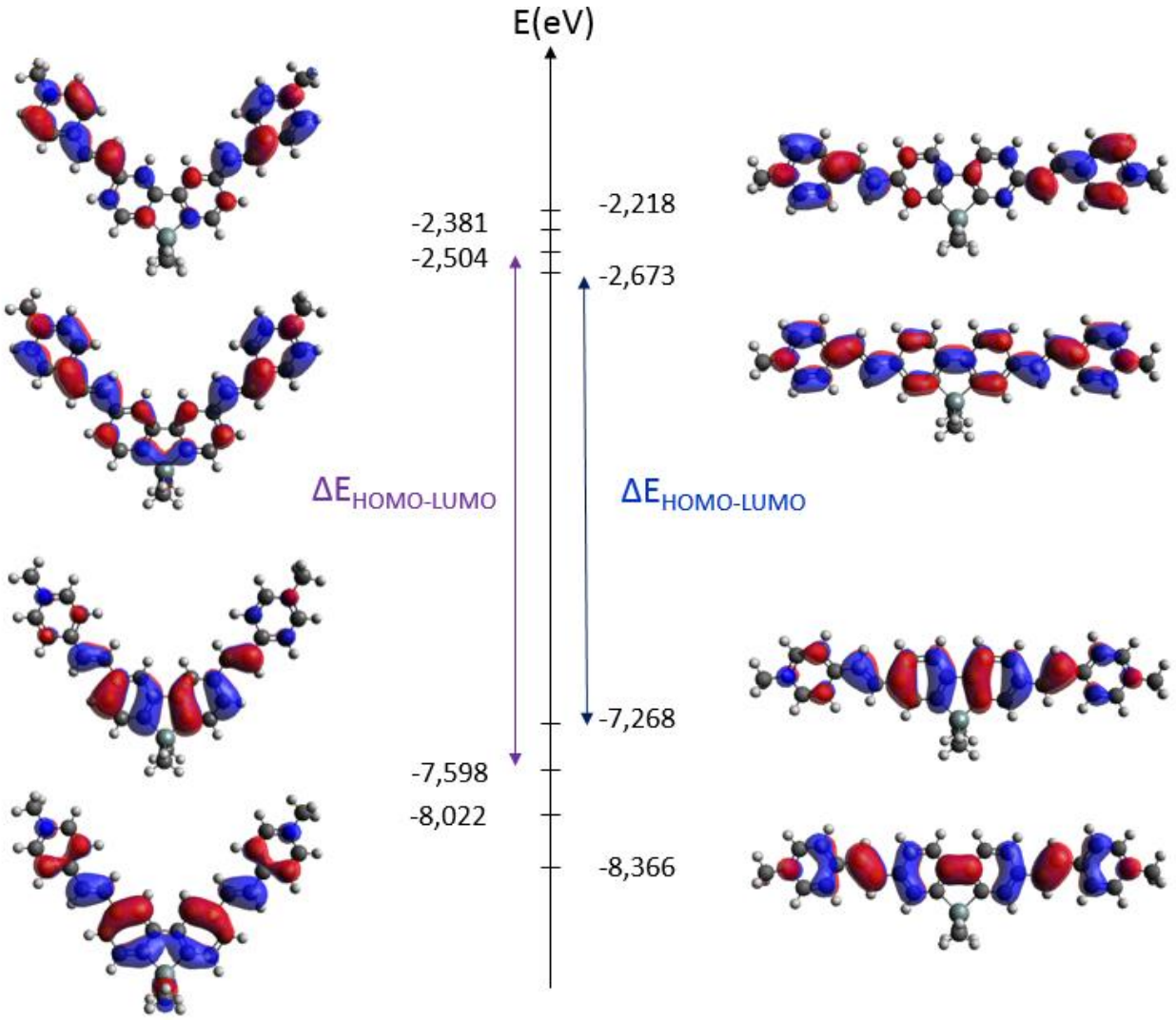

Figure 4. Frontiers orbitals of **SiFluo-L** and **SiFluo-V**

A calculation of the variation of electronic density during the transition from the ground state to the first excited state was thus performed (Figure 5). The increase of the electronic density is shown in blue whereas the decrease is shown in yellow. The electronic density mostly decreases on the silafluorene core whereas it increases on the two branches. It is typical for an internal charge transfer and it is consistent with a A-π-D-π-A design for both probes.

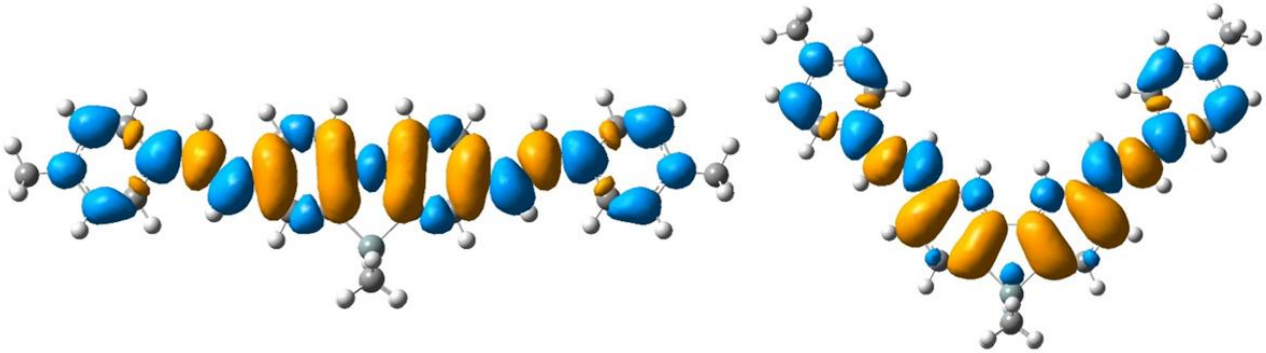

Figure 5. Increase (in blue) and decrease (in yellow) of the electronic density during $S_0 \rightarrow S_1$

Two-photon absorption properties are highly dependent of extension of conjugation and charge transfer; and can thus be related to transition dipole moments. [33-34] Indeed, in the case of centrosymmetric compound and when S2 is the final state, δ_{MAX} is proportional to $\mu_{S0\rightarrow S1}$ and $\mu_{S1\rightarrow S2}$ according to formula (1).

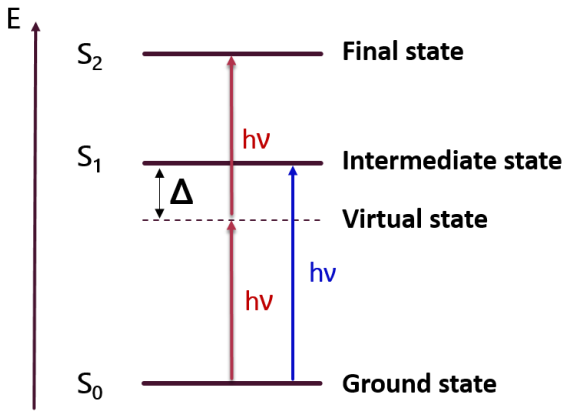

$$\delta_{MAX} \propto \frac{\mu^2_{S_0\rightarrow S_1} \times \mu^2_{S_1\rightarrow S_2}}{\Delta^2} \quad (1)$$

Figure 6. Jablonski diagram for centrosymmetric compounds (1PA in blue, 2PA in red) and relationship between maximal two-photon absorption cross-section δ_{MAX} and transition dipole moments

To explain their difference in two-photon absorption properties, a calculation of the transition dipole moments $\mu_{S_0\rightarrow S_1}$ and $\mu_{S_1\rightarrow S_2}$ was therefore conducted. For both transitions $S_0 \rightarrow S_1$ and $S_1 \rightarrow S_2$ the norm of the transition dipole moment is about twice higher for **SiFluo-L** than **SiFluo-V** (Table 3 and Tables S2 and S3). As a consequence, the calculated δ_{MAX} is 16 times higher for **SiFluo-L**. This is in line with the respective 2PA cross sections of the compounds. Thus, theoretical calculations support the experimental evidence that **SiFluo-L** displays by far better two-photon absorption properties than **SiFluo-V**.

Compound	$\mu_{S_0\rightarrow S_1}$	$\mu_{S_1\rightarrow S_2}$	Δ (eV)	$\frac{\mu^2_{S_0\rightarrow S_1} \times \mu^2_{S_1\rightarrow S_2}}{\Delta^2}$
SiFluo-V	3.47	3.02	2.09	25
SiFluo-L	6.05	5.54	1.66	408

Table 3. Transition dipole moments of **SiFluo-V** and **SiFluo-L** for $S_0 \rightarrow S_1$ and $S_1 \rightarrow S_2$

3.5 Confocal microscopy

First, the biocompatibility of **SiFluo-V** and **SiFluo-L** was evaluated by MTT assay in A549 cells (SI, Figure S4). The probes show no significant effects on cell viability (more than 80% of viable A549 cells at 10 µM) and can be used for live cell imaging. The ability of these two probes for live cells imaging was evaluated through confocal microscopy. After 2h of incubation in A549 cells at 2 µM, images were acquired after one or two-photon excitation.

SiFluo-L exhibits high brightness and contrast at low power of laser under one photon excitation but also under 2PE (3.4 mW laser power) (Figure 7). This value is considered far below the standard noninvasive *in vivo* two-photon studies.[35-36] As expected, no autofluorescence was detected at this power (SI, Figure S5).

We took advantage of this high brightness to reduce the concentration of **SiFluo-L** for live cell imaging. We were able to perform two-photon fluorescence microscopy at only 100 nM increasing laser power to 20 mW (SI, Figure S6).

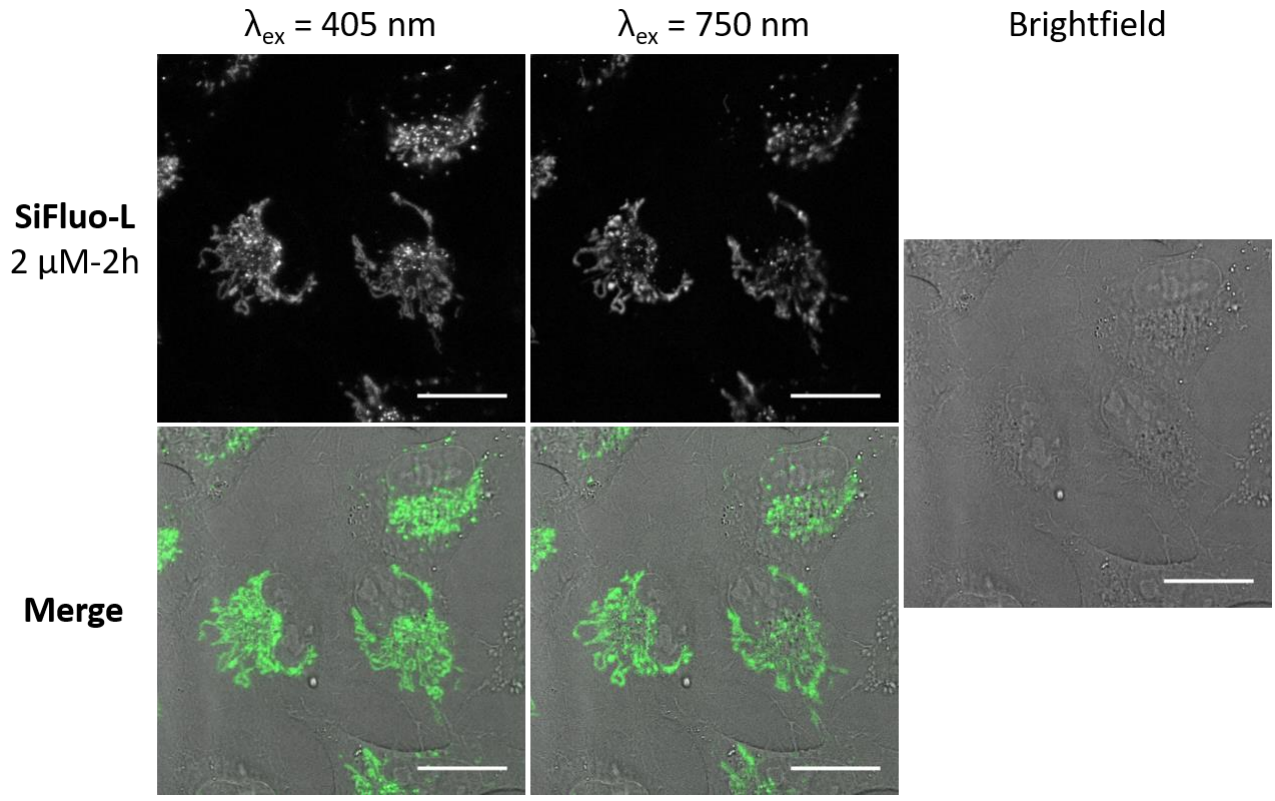

Figure 7. Confocal microscopy imaging of live A549 cells incubated with **SiFluo-L** at 2 µM during 2h under one (405 nm) or two-photon excitation (750 nm). Emission slit settings: 500-650 nm. Scale bar: 20 µm

At the opposite, under one photon excitation, **SiFluo-V** exhibits only moderate brightness and contrast (SI, Figure S7). The poor absorbance of **SiFluo-V** at 405 nm, the lowest excitation laser on the used confocal microscope, can explain this weak fluorescence. Similarly, the poor two-photon brightness at 705 nm (below 60 GM) does not provide high signal-to-noise ratio images.

These two dyes are localized in the cytoplasm as shown by the brightfield images. To confirm this subcellular localization, we performed a colabeling experiment with **SiFluo-L** and DRAQ5, a nuclear stainer (Figure 8). Excitation at 633 nm led to the near infra-red fluorescence of DRAQ5 although excitation at 405 nm led to a green to red fluorescence of **SiFluo-L**. This experiment strongly supports the cytoplasmic localization of **SiFluo-L**. As lipophilic cations are sequestered in mitochondria due to the mitochondrial membrane potential, **SiFluo-L** was expected to label mitochondria. A colocalization was performed with a commercially available tracker (Mitotracker Deep Red, λ_{ex} = 633 nm) to confirm its subcellular localization (Figure 8). The Van Steensel's cross correlation method highlights an overlay between signals from Mitotracker Deep Red and **SiFluo-L**, that confirms its mitochondrial intracellular labeling (SI, Figure S8).

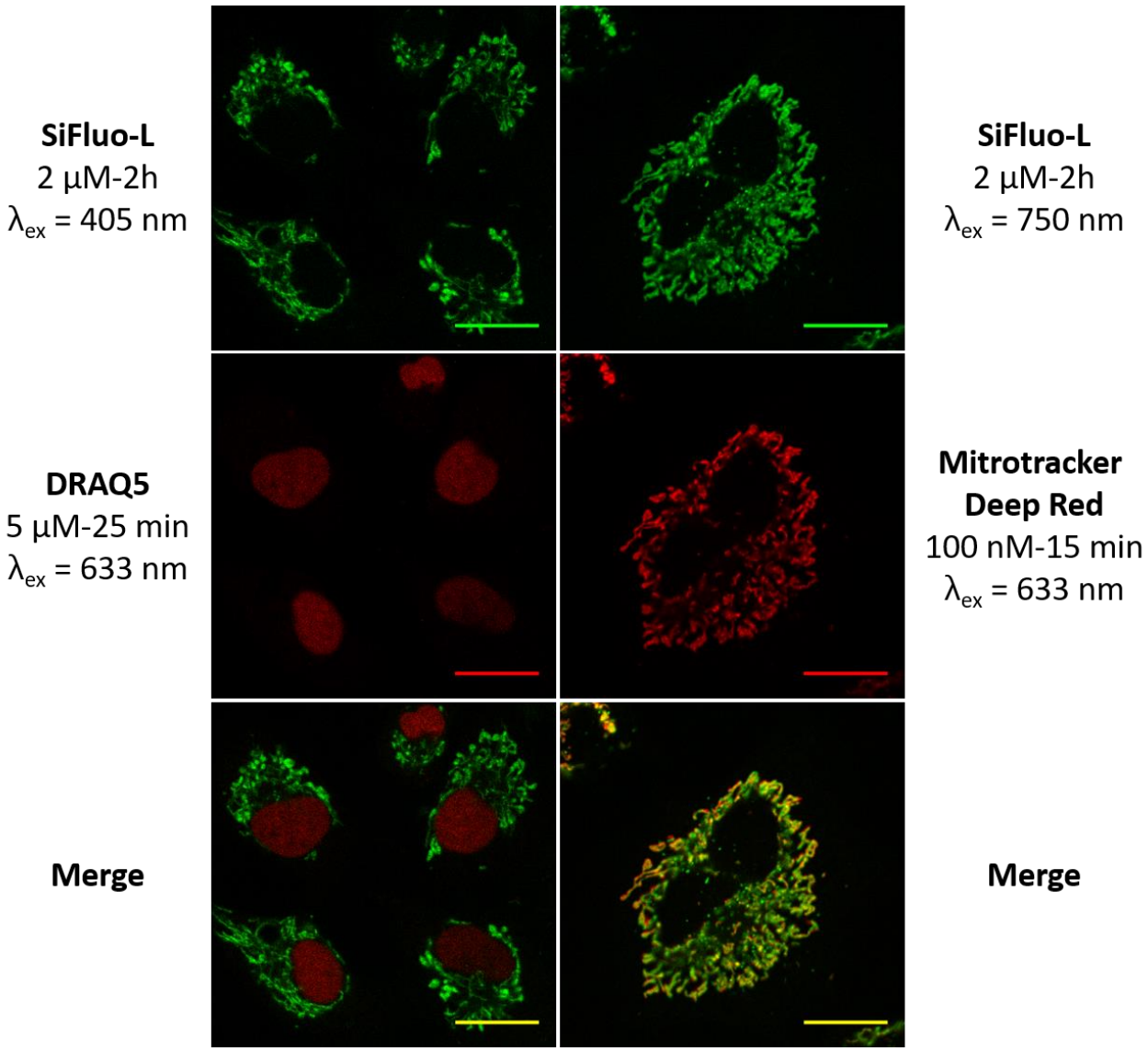

Figure 8. Subcellular localization of **SiFluo-L** (2 µM, 2h, λ_{ex} = 405 nm (left), 750 nm (right) Emission slits settings: 500-700 nm): colabeling with DRAQ5 (5 µM, 25 min, λ_{ex} = 633 nm, Emission slits settings: 650-795 nm) and Mitrotracker Deep Red (100 nM, 15 min λ_{ex} = 633 nm, Emission slits settings: 650-700 nm). Scale bar: 20 µm

SiFluo-L displays a large emission spectra from green to red emission. Due to its high brightness, its emission can be efficiently detected in the red window, from 600 to 700 nm (SI, Figure S9). This NIR emission could be of great interest for *in vivo* imaging.

In addition, these two compounds are highly photostable. After a 10-min acquisition under two-photon excitation, more than 95 % of the fluorescence signal remains for **SiFluo-V** and about 80 % for **SiFluo-L** (Figure 9 and SI, Figure S10).

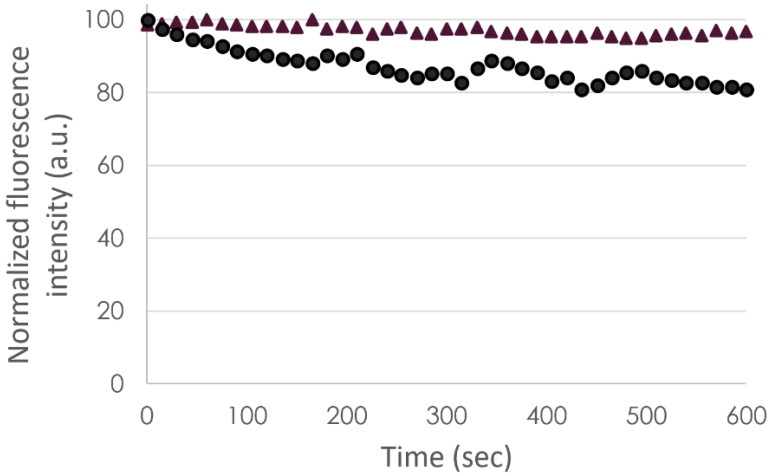

Figure 9. Two-photon photostability of **SiFLuo-V** (triangle) and **SiFluo-L** (round) - λ_{ex} = 705 nm and 750 nm respectively

Conclusion

We designed and synthesized two fluorophores based on a silafluorene core **SiFluo-V** and **SiFluo-L**. These two dyes display a strong fluorescence between 450 and 650 nm, despite of their difference in absorption ranges. **SiFluo-L** exhibits impressive two-photon cross sections (up to 2150 GM) about three times higher than the corresponding fluorene. Thanks to its cell permeability, water solubility and low cytotoxicity (IC_{80}≥10 µM), **SiFluo-L** is a biocompatible dye. The outstanding combination of optical (high two-photon brightness and photostability) and biological properties makes **SiFluo-L** an efficient probe for live cell imaging. As it exhibits a large emission spectrum, we were able to perform cellular imaging in the red window (600-700 nm). This should enable the use of **SiFluo-L** for *in vivo* labeling experiments. The subcellular localization of this probe was shown to be mitochondrial thanks to colocalization experiments. As silafluorene is a promising core for live cell imaging, next step will be to increase its scope by labeling other organelles. Indeed, there is a real need to design probes suitable to label organelles such as Golgi apparatus or endoplasmic reticulum. [4] Modification of the acceptor moieties or addition of targeted organelle moieties on the silafluorene core should be envisaged to ensure the design of new fluorophores for different organelle labeling.

Acknowledgements

M. A. thanks the Ministère de l'Enseignement Supérieur et de la Recherche for her doctoral fellowship. The authors greatly acknowledge the Multimodal Imaging Center-Light Microscopy Facility (Institut Curie, CNRS UMS2016, Inserm US43, Université Paris-Saclay) and particularly Laetitia Besse and Marie-Noëlle Soler for their technical assistance in the use of the Leica confocal SP5 system. This work has benefited from the facilities and expertise of the Small Molecule Mass Spectrometry platform of ICSN (Centre de Recherche de Gif - www.icsn.cnrs-gif.fr).

References

1. Klymchenko, A. S., Solvatochromic and Fluorogenic Dyes as Environment-Sensitive Probes: Design and Biological Applications. *Accounts of chemical research* **2017,** *50* (2), 366-375.
2. Xu, W.; Zeng, Z.; Jiang, J.-H.; Chang, Y.-T.; Yuan, L., Discerning the Chemistry in Individual Organelles with Small-Molecule Fluorescent Probes. *Angewandte Chemie International Edition* **2016,** *55* (44), 13658-13699.
3. Gao, P.; Pan, W.; Li, N.; Tang, B., Fluorescent probes for organelle-targeted bioactive species imaging. *Chemical science* **2019,** *10* (24), 6035-6071.
4. Zhu, H.; Fan, J.; Du, J.; Peng, X., Fluorescent Probes for Sensing and Imaging within Specific Cellular Organelles. *Accounts of chemical research* **2016,** *49* (10), 2115-2126.
5. Stringari, C.; Abdeladim, L.; Malkinson, G.; Mahou, P.; Solinas, X.; Lamarre, I.; Brizion, S.; Galey, J. B.; Supatto, W.; Legouis, R.; Pena, A. M.; Beaurepaire, E., Multicolor two-photon imaging of endogenous fluorophores in living tissues by wavelength mixing. *Scientific reports* **2017,** *7* (1), 3792.
6. Kim, H. M.; Cho, B. R., Small-molecule two-photon probes for bioimaging applications. *Chem Rev* **2015,** *115* (11), 5014-55.

7. Zyss, J.; Ledoux, I., Nonlinear optics in multipolar media: theory and experiments. *Chemical Reviews* **1994,** *94* (1), 77-105.
8. Chung, S.-J.; Kim, K.-S.; Lin, T.-C.; He, G. S.; Swiatkiewicz, J.; Prasad, P. N., Cooperative Enhancement of Two-Photon Absorption in Multi-branched Structures. *The Journal of Physical Chemistry B* **1999,** *103* (49), 10741-10745.
9. Katan, C.; Tretiak, S.; Werts, M. H. V.; Bain, A. J.; Marsh, R. J.; Leonczek, N.; Nicolaou, N.; Badaeva, E.; Mongin, O.; Blanchard-Desce, M., Two-Photon Transitions in Quadrupolar and Branched Chromophores: Experiment and Theory. *The Journal of Physical Chemistry B* **2007,** *111* (32), 9468-9483.
10. Carter, K. P.; Young, A. M.; Palmer, A. E., Fluorescent sensors for measuring metal ions in living systems. *Chem Rev* **2014,** *114* (8), 4564-601.
11. Jiao, X.; Li, Y.; Niu, J.; Xie, X.; Wang, X.; Tang, B., Small-Molecule Fluorescent Probes for Imaging and Detection of Reactive Oxygen, Nitrogen, and Sulfur Species in Biological Systems. *Analytical chemistry* **2018,** *90* (1), 533-555.
12. Peveler, W. J.; Algar, W. R., More Than a Light Switch: Engineering Unconventional Fluorescent Configurations for Biological Sensing. *ACS chemical biology* **2018,** *13* (7), 1752-1766.
13. Rosania, G. R.; Lee, J. W.; Ding, L.; Yoon, H.-S.; Chang, Y.-T., Combinatorial Approach to Organelle-Targeted Fluorescent Library Based on the Styryl Scaffold. *Journal of the American Chemical Society* **2003,** *125* (5), 1130-1131.
14. Xie, X.; Choi, B.; Largy, E.; Guillot, R.; Granzhan, A.; Teulade-Fichou, M. P., Asymmetric distyrylpyridinium dyes as red-emitting fluorescent probes for quadruplex DNA. *Chemistry* **2013,** *19* (4), 1214-26.
15. Naud-Martin, D.; Martin-Benlloch, X.; Poyer, F.; Mahuteau-Betzer, F.; Teulade-Fichou, M. P., Acri-2,7-Py, a bright red-emitting DNA probe identified through screening of a distyryl dye library. *Biotechnology journal* **2014,** *9* (2), 301-10.
16. Dumat, B.; Bordeau, G.; Faurel-Paul, E.; Mahuteau-Betzer, F.; Saettel, N.; Bombled, M.; Metge, G.; Charra, F.; Fiorini-Debuisschert, C.; Teulade-Fichou, M. P., N-phenyl-carbazole-based two-photon fluorescent probes: strong sequence dependence of the duplex vs quadruplex selectivity. *Biochimie* **2011,** *93* (8), 1209-18.
17. Allain, C.; Schmidt, F.; Lartia, R.; Bordeau, G.; Fiorini-Debuisschert, C.; Charra, F.; Tauc, P.; Teulade-Fichou, M.-P., Vinyl-Pyridinium Triphenylamines: Novel Far-Red Emitters with High Photostability and Two-Photon Absorption Properties for Staining DNA. *Chembiochem : a European journal of chemical biology* **2007,** *8* (4), 424-433.
18. Egawa, T.; Hanaoka, K.; Koide, Y.; Ujita, S.; Takahashi, N.; Ikegaya, Y.; Matsuki, N.; Terai, T.; Ueno, T.; Komatsu, T.; Nagano, T., Development of a far-red to near-infrared fluorescence probe for calcium ion and its application to multicolor neuronal imaging. *Journal of the American Chemical Society* **2011,** *133* (36), 14157-9.
19. Kushida, Y.; Nagano, T.; Hanaoka, K., Silicon-substituted xanthene dyes and their applications in bioimaging. *The Analyst* **2015,** *140* (3), 685-95.
20. Lukinavičius, G.; Umezawa, K.; Olivier, N.; Honigmann, A.; Yang, G.; Plass, T.; Mueller, V.; Reymond, L.; Corrêa Jr, I. R.; Luo, Z.-G.; Schultz, C.; Lemke, E. A.; Heppenstall, P.; Eggeling, C.; Manley, S.; Johnsson, K., A near-infrared fluorophore for live-cell super-resolution microscopy of cellular proteins. *Nature Chemistry* **2013,** *5*, 132.
21. Mao, Z.; Jiang, H.; Song, X.; Hu, W.; Liu, Z., Development of a Silicon-Rhodamine Based Near-Infrared Emissive Two-Photon Fluorescent Probe for Nitric Oxide. *Analytical chemistry* **2017,** *89* (18), 9620-9624.
22. Chan, K. L.; McKiernan, M. J.; Towns, C. R.; Holmes, A. B., Poly(2,7-dibenzosilole): A Blue Light Emitting Polymer. *Journal of the American Chemical Society* **2005,** *127* (21), 7662-7663.
23. Liu, X.-Y.; Tian, Q.-S.; Zhao, D.; Ran, Q.; Liao, L.-S.; Fan, J., 9-Silafluorene and 9-germafluorene: novel platforms for highly efficient red phosphorescent organic light-emitting diodes. *Journal of Materials Chemistry C* **2018,** *6* (30), 8144-8151.
24. Chen, S. F.; Tian, Y.; Peng, J.; Zhang, H.; Feng, X. J.; Zhang, H.; Xu, X.; Li, L.; Gao, J., Synthesis and characterization of arylamino end-capped silafluorenes for blue to deep-blue organic light-emitting diodes (OLEDs). *Journal of Materials Chemistry C* **2015,** *3* (26), 6822-6830.
25. Li, L.; Xu, C.; Li, S., Synthesis and photophysical properties of highly emissive compounds containing a dibenzosilole core. *Tetrahedron Letters* **2010,** *51* (4), 622-624.
26. Chan, K. L.; Watkins, S. E.; Mak, C. S.; McKiernan, M. J.; Towns, C. R.; Pascu, S. I.; Holmes, A. B., Poly(9,9-dialkyl-3,6-dibenzosilole)--a high energy gap host for phosphorescent light emitting devices. *Chemical communications* **2005,** (46), 5766-8.
27. Brouwer, A. M., Standards for photoluminescence quantum yield measurements in solution (IUPAC Technical Report). *Pure and Applied Chemistry* **2011,** *83* (12), 2213-2228.
28. Crosby, G. A.; Demas, J. N., Measurement of photoluminescence quantum yields. Review. *The Journal of Physical Chemistry* **1971,** *75* (8), 991-1024.
29. Xu, C.; Webb, W. W., Measurement of two-photon excitation cross sections of molecular fluorophores with data from 690 to 1050 nm. *J. Opt. Soc. Am. B* **1996,** *13* (3), 481-491.
30. Makarov, N. S.; Drobizhev, M.; Rebane, A., Two-photon absorption standards in the 550–1600 nm excitation wavelength range. *Opt. Express* **2008,** *16* (6), 4029-4047.

31. Suzuki, Y.; Tenma, Y.; Nishioka, Y.; Kamada, K.; Ohta, K.; Kawamata, J., Efficient Two-Photon Absorption Materials Consisting of Cationic Dyes and Clay Minerals. *The Journal of Physical Chemistry C* **2011,** *115* (42), 20653-20661.
32. Liu, Y.; Meng, F.; Nie, J.; Niu, J.; Yu, X.; Lin, W., Two-photon fluorescent probe for detecting cell membranal liquid-ordered phase by an aggregate fluorescence method. *J Mater Chem B* **2017,** *5* (24), 4725-4731.
33. Rumi, M.; Ehrlich, J. E.; Heikal, A. A.; Perry, J. W.; Barlow, S.; Hu, Z.; McCord-Maughon, D.; Parker, T. C.; Röckel, H.; Thayumanavan, S.; Marder, S. R.; Beljonne, D.; Brédas, J.-L., Structure−Property Relationships for Two-Photon Absorbing Chromophores: Bis-Donor Diphenylpolyene and Bis(styryl)benzene Derivatives. *Journal of the American Chemical Society* **2000,** *122* (39), 9500-9510.
34. Pawlicki, M.; Collins, H. A.; Denning, R. G.; Anderson, H. L., Two-photon absorption and the design of two-photon dyes. *Angewandte Chemie* **2009,** *48* (18), 3244-66.
35. Sacconi, L.; Dombeck, D. A.; Webb, W. W., Overcoming photodamage in second-harmonic generation microscopy: real-time optical recording of neuronal action potentials. *Proc Natl Acad Sci U S A* **2006,** *103* (9), 3124-9.
36. Wang, B. G.; Konig, K.; Halbhuber, K. J., Two-photon microscopy of deep intravital tissues and its merits in clinical research. *J Microsc* **2010,** *238* (1), 1-20.